DOI: 10.13009/EUCASS2025-680
11TH EUROPEAN CONFERENCE FOR AERONAUTICS AND SPACE SCIENCES (EUCASS)

Effect of collector shape in the performance of EAD thrusters

Marco Belan ⋆ † *Raffaello Terenzi* ⋆ *Stefano Trovato* ⋆ *Davide Usuelli* ⋆
⋆ *Department of Aerospace Science and Technology, Politecnico di Milano, Milan, Italy*
Via La Masa 34, 20156, Milano
marco.belan@polimit.it · raffaello.terenzi@polimi.it
†Corresponding author

Abstract

This work presents a comprehensive multiparameter experimental investigation aimed at optimizing the performance of electro-aerodynamic (EAD) corona thrusters through the combined effects of geometrical parameters and emitter configurations. A physically consistent scaling model is used to define reference values and dimensionless performance indicators such as thrust and thrust-to-power coefficients (C_T, C_{TP}). The campaign explores a wide parameter space, testing airfoil and droplet collectors of varying chord lengths and thicknesses arranged in parallel arrays at different spacings. Additionally, the impact of emitter configuration—collinear versus staggered—on performance is evaluated. Direct thrust and electrical measurements are used to extract key performance coefficients. Results indicate that nonuniform, staggered emitter arrangements combined with short chord, adequately thick collectors significantly enhance performance, with droplet-shaped collectors showing competitive behavior compared to traditional airfoils. Optimal configurations are identified for maximizing C_T and C_{TP}, offering valuable design insights for next-generation EAD propulsion systems.

1. Introduction

The demand for sustainable aviation has driven worldwide researchers over the past decades to seek alternative propulsion methods to conventional aeronautical thermal engines.[1,2] The current trend is to develop electrical propulsion systems to reduce pollutants and noise around airports and major cities. Historically, electric propulsion has been used in space applications such as in Hall thrusters,[3–5] while electric-driven propellers are utilized for UAVs and small general aviation planes. A promising alternative to propellers are electro-aerodynamic (EAD) thrusters. These devices, characterized by their simple geometry, offer advantages such as zero emissions, low noise and no moving parts, resulting in reduced maintenance requirements. Notable prototypes include aeroplane[6] which glided thrown by a slingshot, and ionocrafts[7] which lifted vertically with a wireless power supply on board. These prototypes, dating back a decade ago, demonstrated the feasibility of EAD technology.

An EAD thruster, depicted in its simplest form in Figure 1, consists of two electrodes operating under a corona discharge regime: the emitter - where air ionization occurs - and the collector. The electrodes are supplied with a high voltage source, creating an intense electric field that promotes ionization near the emitter and drifts ions towards the collector.[8,9] The ion emitter is in general characterized by a small cross section: wires with a diameter below 200 μm are often employed, however other geometries such as blades[10–12] and pins[13–15] are also found in literature. The collector unit features a greater dimension, with airfoils,[6] cylinders[16] and droplets[7] being the adopted geometries: several studies involving their optimization can be found in literature.[17–19] The generated thrust results from the interaction between drifting ions and neutral molecules, which exchange momentum during collisions. A basic EAD thruster consists of a single emitter and collector, forming a thruster unit. Thruster arrays can be generated by stacking units in parallel[18,20] or aligning them sequentially to form multi-staged thrusters.[19,21]

The spatial arrangement of electrodes is still subject to investigation, leading to different concepts. Studies in the literature focus on optimizing the distance between collectors *SC* and the distance *d* between electrodes of opposed polarity for a given voltage and electrodes shape. Given that this technology is still in its early stages of development, there is significant room for improvement. One of the open fields of investigation is the arrangement of emitters, such as increasing their density,[22] which proportionally enhances multiple performance parameters until the occurrence of the shielding phenomenon, leading to performance degradation.[23,24] In general, EAD thrusters operate using a DC voltage supply for the corona discharge; however, different ionization sources can be employed, such as DBD[25,26] which exploits the AC regime or nanosecond pulsed power supplies, capable of generating an increased amount of ions before breakdown occurs.[27,28] Thrusters have been tested both on the bench and in wind tunnels to investigate the

DOI: 10.13009/EUCASS2025-680

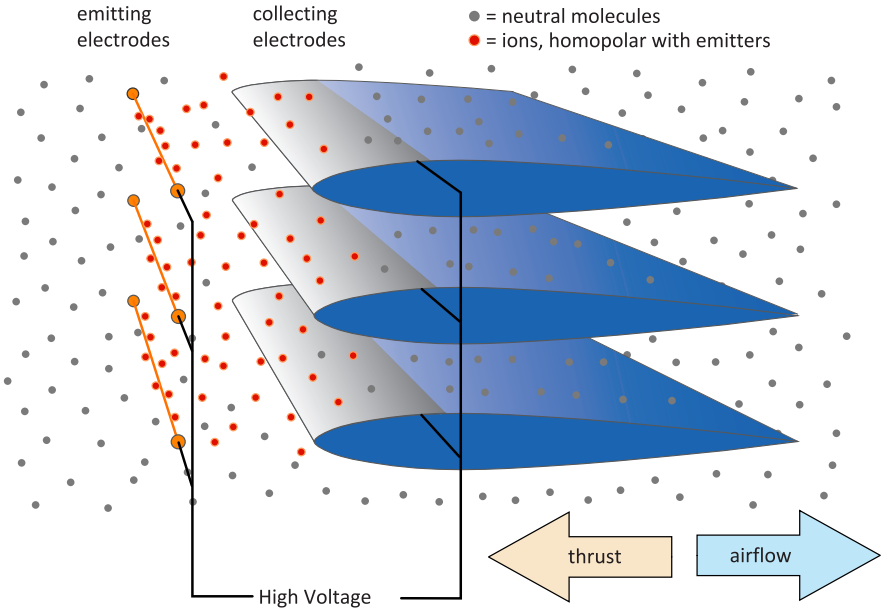

Figure 1: Schematic representation of an EAD thruster.

effects of an asymptotic flow.[29–31] The performance of an EAD thruster is typically evaluated considering the generated thrust (T), Power consumption (P), Thrust-to-Power ratio (T/P) as an efficiency index and thrust density (T/A) as a compactness index, with A being the reference frontal area. The promising performance of EAD thrusters has also attracted interest from airship designers[32] for potential low-cost alternatives to satellites.
In this paper, two experimental campaigns are presented. The primary design variable of the first work is the shape of the collectors, identifying the thickness and the chord as the main parameters which are used to generate a corresponding NACA 4-digit airfoil. In the second work, the focus is on emitter arrangement and how it affects performances on airfoil and drop-shaped collectors.

2. Design of experiment

2.1 Parameter space

The first work investigates the effect of thickness and chord length of a NACA 4 digit airfoil on the performance of an EAD thruster with the parameter space shown in Figure 2. The investigated chords are $15, 25, 40$, and 100 . Each chord family presents airfoils with variable thicknesses of $6, 10$, and 14 mm. A further airfoil with chord 25 mm and thickness 2 mm was introduced during the tests to corroborate the experimental trends. Each configuration will be indicated using the notation $CxxTyy$, where xx indicates the chord in millimeters and yy the thickness in millimeters. The gap d between electrodes is kept fixed at 20 mm as as the effects of d (and voltage) were already investigated. already investigated in literature. To limit the variable space of the investigation some variables are kept constant: applied voltage V_a = 20kV, spacing between collectors SC= 35 mm and collinear electrodes, namely the emitter and collector are aligned such that their central axes lie on a common straight line.
In the second work, the parameter space is reduced around the region of optimum from previous work. The thickness to chord ratio t/c is fixed at 24% while chord varies as $c = 15, 20, 25$ mm. Contrary to previous work, both airfoil and drop-shaped collectors are tested as both proved to be a valid solution in literature. The same nomenclature presented before is utilized. A further investigation introduced here is related to emitter arrangement as their disposition affects ignition voltage and ion generations hence thrust and current. Five different emitters configurations are tested and described by Figure 3, as well as employing differently shaped collectors.

2.2 Performance coefficients

The experimental data are analyzed in order to generate performance indicators, useful for comparing the results deriving from the different configurations. In literature, three performance parameters are generally adopted: the

DOI: 10.13009/EUCASS2025-680

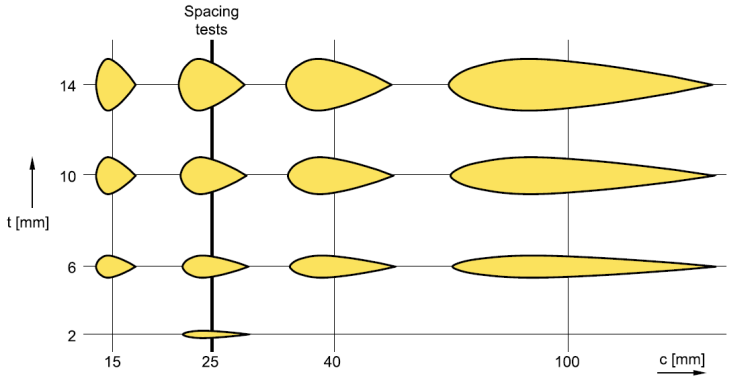

Figure 2: Parameter space of airfoils collectors

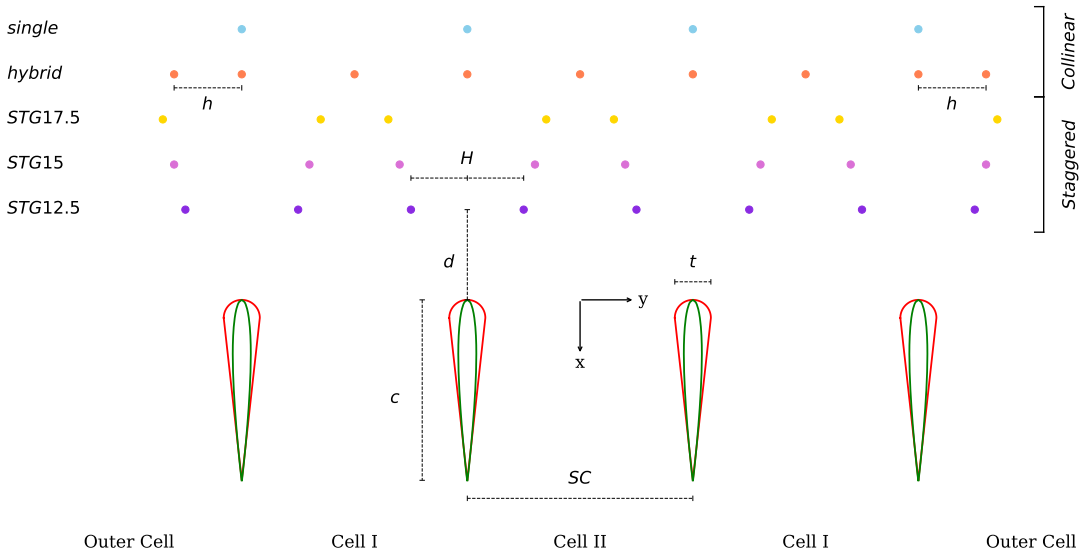

Figure 3: Geometrical definition and nomenclature, not to scale. Red sketch represents droplet collectors, green represents airfoil collectors. From Usuelli et al.[33]

generated thrust T, the Thrust-to-Power ratio T/P and the thrust density T/A. Depending on the optimization target, these parameters can be exploited to generate Pareto fronts for tradeoff analyses. In this work, T and T/P are the main outputs of interest: in order to provide meaningful comparisons with other setups, their dimensionless counterparts are introduced. The complete derivation can be found in Kahol et al.[17] : the respective coefficients for T and T/P are reported in Table 1, where ϵ is the permittivity and μ_q the ion mobility. Each coefficient is obtained dividing the dimensional data by the corresponding reference value.

3. Experimental setup

The test rig utilized in both experimental campaign shares common features. Components are produced via rapid prototyping using Acrylic Styrene Acrylonitrile (ASA). The setup consists of three main parts: the emitter frame, the collector frame and structural beams. An example is shown in Figure 4.

Constantan wires with a diameter of 30 μm act as emitters. A long wire is wound around lateral arrays of pegs to form an array of parallel emitters. The spacing SE between the emitters is adjustable, starting from a minimum of 2.5 mm. Emitters are connected to the positive pole of a DC high voltage power supply. On the collector frame, holders are designed in order to accommodate various geometries. Four collectors are mounted in each test, as shown

DOI: 10.13009/EUCASS2025-680

Table 1: Performance parameters and dimensionless coefficients.

	Symbol	Ref. value from[17]	Coefficient
Thrust	$\frac{T}{b}$	$\epsilon\frac{V_c^2}{d}$	C_T
Thrust-to-Power	$\frac{T}{P}$	$\frac{d}{\mu_q V_c}$	C_{TP}

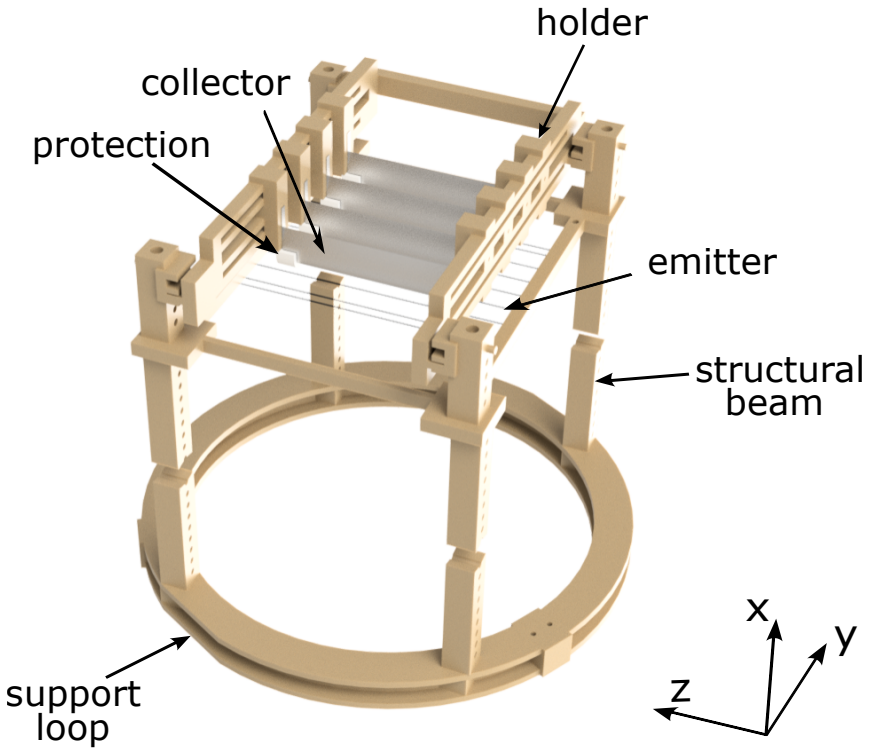

Figure 4: Experimental rig.

in the figure, these include airfoil and droplet geometries with variable thickness t and chord c. Each collector is coated with a 70 μm thick aluminium foil and is electrically grounded. Insulating caps protect the ends of the collectors that face the emitters, in order to prevent reverse corona and early streamer formation due to the electric field intensity in this area. The collector holder allows for adjustable spacing between electrodes SC starting from a minimum of 10 mm.

3.1 Thrust measurement

Thrust measurement is the main technique used in this experimental campaign to characterize the performances of the thruster's different configurations. The setup described above is positioned on top of a precision balance, characterized by a 0.1 mN accuracy. Structural beams ensure adequate spacing between electrodes and the balance plate to prevent electrostatic interference, an additional grounded plate is placed on top of the balance for the same reason. In all experiments the distance between the downward facing emitters and the balance plate is always greater than 400 mm.

3.2 Electrical measurement

The electrical scheme of the setup is shown in Figure 5. Both setups share the same high voltage power supply which provides a positive DC voltage $V_s = 20 \pm 0.03$ kV. A ballast resistance $R_b = 0.996 \pm 0.003$ MΩ has been introduced

DOI: 10.13009/EUCASS2025-680

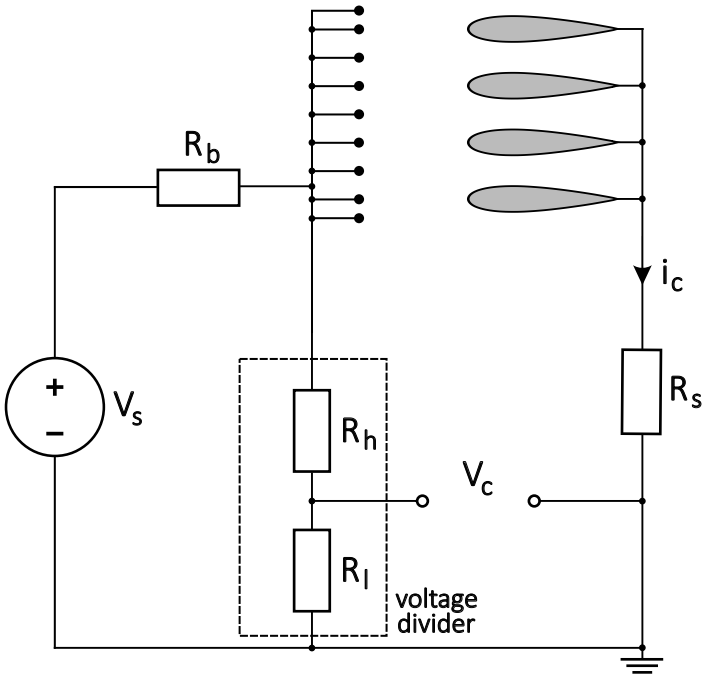

Figure 5: Electrical scheme.

for safety purposes. During the tests, corona voltage V_c and current i_c across the electrodes are measured. The former is acquired using a voltage divider with $R_{tot} = 47 \pm 0.001$ MΩ, while the latter is obtained from the voltage signal read across a $R_s = 88.5 \pm 0.01$ Ω shunt resistor.

3.3 Data acquisition

During the thrust measurement, the thrust T is determined by the difference in the balance output reading when the thrust is switched on and off. For each test, acquisitions are averaged to obtain the final values, while the uncertainty are propagated using the Root Sum of Squares (RSS) method. Thrust, V_c and i_c are acquired using an oscillope with an acquisition time of 2 s and sampling frequency of 50 kS/s.

4. Results

The effect of the chord and of the thickness on the performance of the thruster is here presented in terms of C_T and C_{TP} as shown in Figure 6.

Performance levels are a trade off between electrical and fluid dynamics properties. On one hand, increasing the thickness has a beneficial effect on the generated electrical thrust since the discharge section increases. On the other hand, an increase in thickness raises the t/c ratio, which makes the airfoil and therefore the collector less aerodynamic; moreover, it decreases the collector spacing-to-thickness ratio, causing an increased worsening of the aerodynamic performance due to blockage effects. The combination of these effects results in the presence of a local maximum as a function of thickness for a given chord. Both the $C100$ and $C40$ families present this maximum in the corresponding $T10$ airfoil, while the $T14$ airfoil suffers from blockage effects. The $C25$ family presents this maximum in the $T6$ airfoil, since the $C25T10$ airfoil has a shape with poor aerodynamic characteristics, given its 40% thickness-to-chord ratio. The local maximum for the $C15$ chord family should presumably appear on the left, outside the investigated parameter space, but its practical implementation may be prohibitively complex. Overall, the global maximum for C_T in the parameter space is represented by the $C25T6$ airfoil. As for thrust-to-power, C_{TP} reflects the combination of all the effects mentioned so far. It is interesting to observe that, as the chord is decreased, there is a slight increase in C_{TP} followed by a decrease.

DOI: 10.13009/EUCASS2025-680

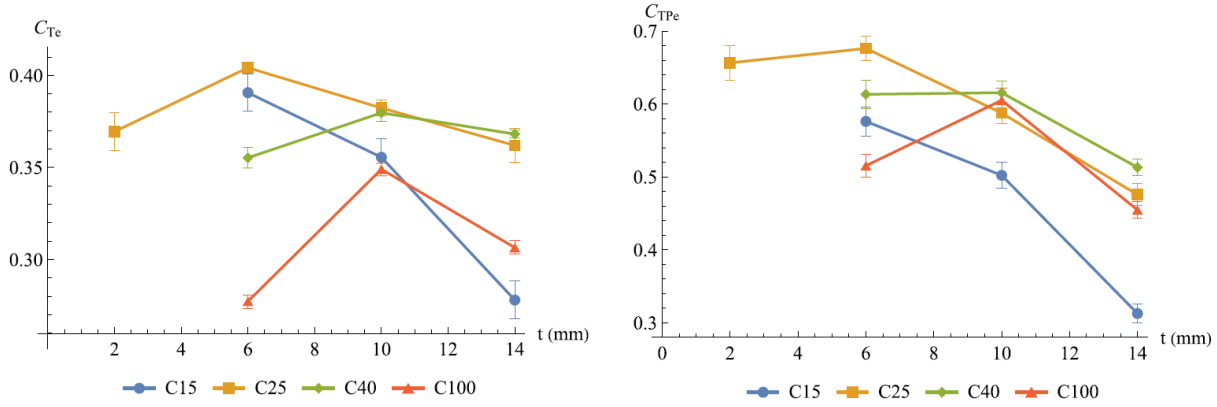

(a) C_T (b) C_{TP}

Figure 6: Performance coefficients as a function of thickness and chord from Kahol et al.[17]

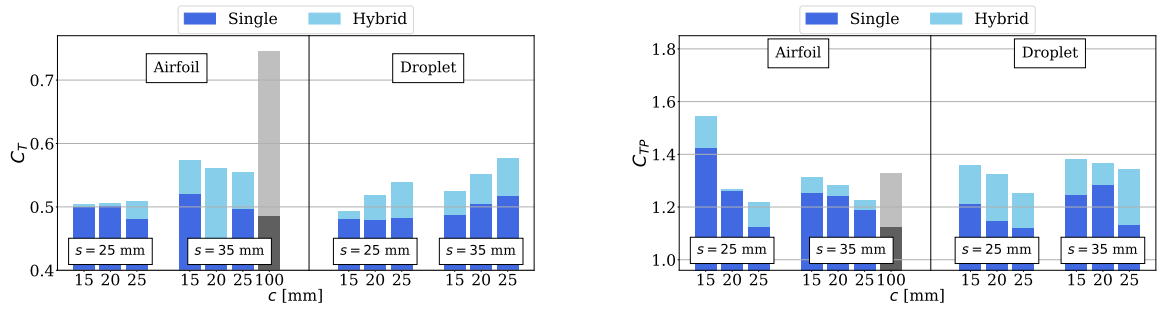

(a) C_T (b) C_{TP}

Figure 7: Performance comparison of *single* and *hybrid* configurations from Usuelli et al.[33] Data for C100 airfoils from previous work are reported for comparison.

An airfoil with $c = 25$ mm and $t = 6$ mm, which corresponds to $t/c = 24\%$, serves as the baseline geometry for the second experimental campaign. Five different emitter arrangements are tested on airfoil and drop-shaped collectors as shown in Figure 3, results are shown in Figure 7 and Figure 8. The value of h for *hybrid* configuration is selected after a performance study that identifies $h = 7.5$ mm as the best value. The staggered configuration investigates $H = 12.5, 15, 17.5$ mm.

Each hybrid configuration outperforms the corresponding single arrangement. For the airfoil-shaped collectors, a smaller chord length leads to higher C_T, while the trend is the opposite for droplet collectors. As the size of the collectors decreases, the gain in performance provided by the hybrid disposition is generally reduced. The introduction of external emitters in a thruster with long chord collectors creates a beneficial extra velocity on the lee side of the outer collectors. This advantage is reduced when using short collectors; however, long collectors turn out to be much heavier, limiting their use in viable applications. Therefore, they are excluded from further considerations in the following sections. The limited increase in performance provided by the hybrid arrangement suggests that this emitter configuration is less effective on small collectors.

In the staggered configurations, only two emitters per collector are placed, since increasing the number with small spacings may easily lead to electric shielding, while increasing the spacing results in performance degradation. The histogram plot of Figure 8 illustrates that the STG15 configuration provides the highest thrust coefficients C_T for both airfoil and droplet collectors. Moreover, this staggered configuration consistently outperforms the hybrid arrangement in terms of thrust.

Regarding thrust-to-power coefficient C_{TP}, non-uniform arrays exhibit higher values compared to the hybrid configuration, as expected due to the greater average distance between the electrodes near the collectors. However, unlike in the case of the thrust coefficient C_T, no single staggered configuration consistently provides the highest C_{TP} values across all collector types, and the variations remain limited.

DOI: 10.13009/EUCASS2025-680

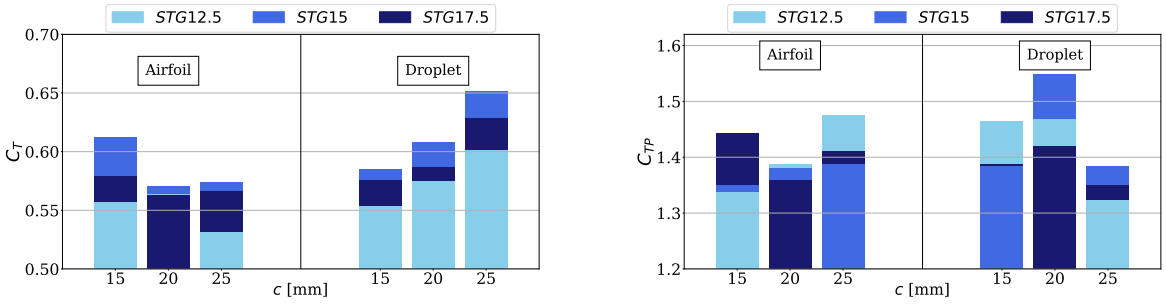

(a) C_T (b) C_{TP}

Figure 8: Performance comparison between staggered configurations from Usuelli et al.[33] The $STG15$ arrangement provides the highest values for C_T, while all staggered configurations deliver similar performances in terms of C_{TP}.

5. Conclusions

This work presents a detailed analysis of the effects of the main geometrical parameters of corona thrusters, with particular focus on the thickness and chord of airfoil-shaped collectors. The total generated thrust was directly measured using precision load cells, alongside electrical data such as current. The results show that reducing the collector chord is beneficial, as shorter airfoils experience less parasitic drag. However, the collector thickness must be carefully selected to balance aerodynamic efficiency and electrical performance: while thinner collectors improve aerodynamics, a sufficient discharge section enabled by greater thickness is essential for effective ion generation. Consequently, ratios such as chord-to-gap and thickness-to-chord (or thickness-to-gap) must be optimized concurrently to achieve superior performance.

In a second stage of the investigation, it was found that both airfoil and droplet-shaped collectors provide comparable performance levels. However, the emitter arrangement plays a critical role in determining overall efficiency. In particular, configurations such as staggered and hybrid emitter layouts significantly influence the electric field distribution and resulting thrust characteristics.

Overall, the results highlight that while collector shape and size are important, there remains considerable room for improvement by refining emitter configurations and optimizing geometric ratios. These findings offer valuable insights for the future design of efficient electrohydrodynamic (EHD) thrusters.

Further developments of EAD thrusters include the usage of radically different collectors of the ultra-thin type that should in principle multiply the thruster's performance in terms of generated thrust and thrust-to-weight ratio. These advanced configurations are currently in testing, but preliminary results showed that thrust could in principle double while keeping a similar thrust-to-power.

6. Acknowledgments

This project has received funding from the European Unionâs Horizon Europe Research and Innovation Programme under Grant Agreement No 101098900. Views and opinions expressed are however those of the authors only and do not necessarily reflect those of the European Union or European Innovation Council and SMEs Executive Agency (EISMEA). Neither the European Union nor the granting authority can be held responsible from them.

References

[1] Cao W, Mecrow B C, Atkinson G J, Bennett J W and Atkinson D J 2012 *IEEE Trans. Ind. Electron.* **59** 3523–3531

[2] Brelje B J and Martins J R 2019 *Prog. Aerosp. Sci.* **104** 1–19

[3] Goebel D M and Katz I 2008 *Fundamentals of electric propulsion: ion and Hall thrusters* (John Wiley & Sons, Hoboken, NJ, USA)

[4] Mazouffre S 2016 *Plasma Sources Sci Technol* **25** 033002

[5] Charles C 2009 *J. Phys. D* **42** 163001

DOI: 10.13009/EUCASS2025-680

[6] Xu H, He Y, Strobel K, Gilmore C, Kelley S, Hennick C, Sebastian T, Woolston M, Perreault D and Barrett S 2018 *Nature* **563** 532–535

[7] Khomich V and Rebrov I 2018 *J. Electrost.* **95** 1–12

[8] Townsend J 1914 *Lond. Edinb. Dublin philos. mag. j. sci.* **28** 83–90

[9] Fridman A and Kennedy L 2004 *Plasma Physics and Engineering* (Taylor & Francis)

[10] Wilson J, Perkins H and Thompson W 2009 An investigation of ionic wind propulsion Tech. Rep. NASA/TM-2009-215822 NASA

[11] Belan M, Baldo J, Kahol O and Montenero D 2024 *Journal of Physics D: Applied Physics* **57**

[12] Kaci M, Said H A, Laifaoui A, Aissou M, Nouri H and Zebboudj Y 2015 *Braz. J. Phys.* **45** 643–655

[13] Ieta A and Chirita M 2019 *J. Electrost.* **100** 103352

[14] Drew D and Follmer S 2021 High force density multi-stage electrohydrodynamic jets using folded laser micro-fabricated electrodes *21st International Conference on Solid-State Sensors, Actuators and Microsystems (Transducers), New York* (Inst. of Electrical and Electronics Engineers) pp 54–57

[15] Chirita M and Ieta A 2022 *J. Propuls. Power* **38** 893–900

[16] Moreau E, Benard N, Lan-Sun-Luk J D and Chabriat J P 2013 *J. Phys. D* **46** 475204

[17] Kahol O, Belan M, Pacchiani M and Montenero D 2023 *J. Electrost.* **123** 103815

[18] Belan M, Arosti L, Polatti R, Maggi F, Fiorini S and Sottovia F 2021 *J. Electrost.* **113** 103616

[19] Xu H, Gomez-Vega N, Agrawal D and Barrett S 2019 *J. Phys. D* **53** 025202

[20] Ieta A, Ellis R, Citro D, Chirita M and DâAntonio J 2013 Characterization of corona wind in a modular electrode configuration *Proc. ESA Annual Meeting on Electrostatics* (Cocoa Beach, FL) pp 1–7

[21] Gomez-Vega N and Barrett S R H 2024 *AIAA Journal* **62** 1342–1353

[22] Belan M, Terenzi R, Trovato S and Usuelli D 2022 *J. Electrost.* **120** 103767

[23] Lemetayer J, Marion C, Fabre D and PlourabouÃ© F 2022 *J. Phys. D* **55** 185203

[24] Arif S, Branken D J, Everson R C, Neomagus H W J P and Arif A 2018 *J. Electrostat.* **93** 17–30

[25] Vega N, Xu H, Abel J and Barrett S 2021 *Appl. Phys. Lett.* **118** 074101

[26] Xu H, He Y and Barrett S 2019 *Appl. Phys. Lett.* **114** 254105

[27] OrriÃ¨re T, Ãric Moreau and Pai D Z 2019 *Journal of Physics D: Applied Physics* **52** 464002

[28] Lacoste D, Pai D and Laux C 2004 *Ion Wind Effects in A Positive DC Corona Discharge in Atmospheric Pressure Air* (American Institute of Aeronautics and Astronautics)

[29] Guerra-Garcia C, Nguyen N, Mouratidis T and Martinez-Sanchez M 2020 *Journal of Geophysical Research: Atmospheres* **125** e2020JD032908

[30] Grosse S, Benard N and Moreau E 2024 *Journal of Electrostatics* **130** 103950

[31] Trovato S, Terenzi R, Usuelli D and Belan M 2024 *Journal of Physics D: Applied Physics* **58** 015201

[32] Riboldi C, Belan M, Cacciola S, Terenzi R, Trovato S, DUsuelli and Familiari G 2024 *Aerospace* **11** ISSN 2226-4310

[33] Usuelli D, Terenzi R, Trovato S and Belan M 2024 *IEEE Transactions on Plasma Science* **52** 5414–5421